



Full paper

Self-powered eye motion sensor based on triboelectric interaction and near-field electrostatic induction for wearable assistive technologies

David Vera Anaya^{a,b}, Tianyi He^{c,d,e,f}, Chengkuo Lee^{c,d,e,f}, Mehmet R. Yuce^{a,b,*}^a Department of Electrical and Computer Systems Engineering, Monash University, 14 Alliance Lane, Monash University, Clayton, Victoria, Australia^b Biomedical Integrated Circuits and Sensors Laboratory, 14 Alliance Lane, Monash University, Clayton, Victoria, Australia^c Department of Electrical & Computer Engineering, National University of Singapore, 4 Engineering Drive 3, 117576, Singapore^d National University of Singapore Suzhou Research Institute (NUSRI), Suzhou, Industrial Park, Suzhou, 215123, China^e Hybrid Integrated Flexible Electronic Systems (HIFES), 5 Engineering Drive 1, 117608, Singapore^f Center for Intelligent Sensors and MEMS, National University of Singapore, 4, Engineering Drive 3, 117576, Singapore

ARTICLE INFO

Keywords:

Triboelectric sensor
Eye motion
Wearable HMI
Disabled-people aid
Hands-free computer control

ABSTRACT

Triboelectric nanogenerators show great potential as flexible motion transducers for wearable human-machine interfaces (HMI). The present research explores a new configuration named Non-Attached Electrode-Dielectric Triboelectric Sensor (NEDTS) and its application in specialized HMI to support people with disabilities in daily life. In this topology, the conductive electrodes are not bonded to the dielectric materials by any coating or sputtering process. Instead, due to the triboelectric interaction between the two elements in motion, voltage is generated in a separate conductor by non-contact electrostatic induction. This allows a near field remote sensing using triboelectric/electrostatic coupling. By applying the mentioned sensing technique, an Orbicularis Oculi muscle motion sensor has been developed to monitor voluntary and involuntary eye blinks. The new transducer is integrated into a portable HMI for hands-free computer cursor control to assist people with mobility impairment. The conceived device was also tested in other applications as hands-free remote car and drone control, and for monitoring driving behaviour. Additionally, a PDMS-based eyelid motion sensor has been tested to feature other virtues of the NEDTS when sensing unconventional motion dynamics.

1. Introduction

Contemporary healthcare services increasingly rely on novel wearable and stretchable sensors that aim to continuously monitor human activities as well as physiological signals [1–4]. At the same time, the increase in Internet of Things (IoT) applications has boosted the development of wearable sensors for daily telemonitoring and control [5–7]. In particular, IoT has offered a platform for the assistance of handicapped people by means of specialized HMI (specifically based on EEG, EMG, voice and video signals) and novel IoT network architectures [8, 9]. As explained in Ref. [8] a perception layer for systems intended to assist handicapped individuals, require chips, RFID tags, actuators, and body sensors. Unfortunately, wearable biosensors still pose a challenge related to power consumption and size, leading to novel research for the improvement of the mechanical and electrical properties of bulky wearable electronics [10,11]. Specifically, the emerging Triboelectric

Nanogenerators (TENGs) can potentially solve size and power problems in motion sensors for an optimal contribution of transducers to the growing field of IoT [12]. TENGs show a significant impact on power generation, flexibility, and monitoring, depending on the physical configuration, materials' choice and motion dynamic [11–20]. Triboelectric generators can be arranged as active flexible sensors for acceleration, pressure, liquid volume or airflow monitoring by using configurations such as relative sliding mode, contact-separation mode (CSM), or freestanding mode [21–29]. In addition, TENGs are also used as flexible biosensors for cardiac monitoring, activity monitoring of limbs and fingers, gait recognition, sleep monitoring, fall detection, and driving behaviour assessment [30–42].

On the other hand, cutting-edge HMIs for disabled patients with limited mobility, are mostly controlled by facial expressions, head movement, video sensing, and EMG [43,44]. Recently, eye motion sensors (electrooculography) are also being used to support

* Corresponding author. Department of Electrical and Computer Systems Engineering, Monash University, 14 Alliance Lane, Monash University, Clayton, Victoria, Australia.

E-mail address: mehmet.yuce@monash.edu (M.R. Yuce).

<https://doi.org/10.1016/j.nanoen.2020.104675>

Received 9 January 2020; Received in revised form 4 March 2020; Accepted 5 March 2020

Available online 11 March 2020

2211-2855/© 2020 Elsevier Ltd. All rights reserved.

handicapped people for wheelchair control and external device control [45–47]. Even though literature presents different sensor devices for the above-mentioned HMIs, the new triboelectric sensors (TS) are still not popular among the different sensing methods to help handicapped patients. Although TSs are integrated into HMIs to control drones, toy cars, computer navigation, and digital written communication [48–54], few works have considered TSs in applications to assist disabled people and amputees' daily problems. A few remarkable examples are the glass mounted eye motion TS (replacing conventional electrooculography) for hands-free wireless typing [54] and the breath TENG monitor pictured in a wheelchair control application in Ref. [55].

Moreover, the integration of triboelectric sensors into complete portable electronic systems also poses a challenge for its long term use. Most of the proposed TENG-based sensors mentioned before, still make use of non-portable commercial electrometers, limiting full wearability. Relevant literature shows that few of the developed TENG systems for small motion monitoring [7,55–57] use portable conditioning circuits with adequate input impedance, noise-canceling, and amplification to provide robust wearability features.

Finally, in the majority of the above-mentioned approaches, TENG configurations require the electrodes and dielectrics to be bonded by using electrospinning or sputtering decomposition processes, which seems an unavoidable manufacturing stage [58]. The versatility, applicability, and robustness sometimes are affected when the TENG-to-system link should use a physical interconnect [59], which in the practice can be a wire connected to a non-portable commercial electrometer. To improve this situation, novel configurations have been developed in literature as the Non-Contact TENG mode [26,60,61], where a “tribo surface space” exists between the two dielectric layers or the wireless triboelectric/electrostatic sensor in Ref. [62]. In such development [62], the triboelectric effect and the non-contact electrostatic induction is used in a smart patch for wireless near-field communication and human motion monitoring. The last approach differs from the non-contact TENG since the dielectric layers are in constant friction but the conductive is separated in distance. Such configuration could give more stability to the signal since there is no decay of charge as in the non-contact mode configuration.

The present report proposes and discusses the analysis and experiment results of a new triboelectric sensor integrated into a portable HMI system for handicapped people. The new triboelectric sensor differs from the existing configurations [29] because the assembling step of bonding nanowires or depositing conductive material on the dielectric polymer was eliminated by using a non-attached electrode-dielectric approach (non-contact mode). To demonstrate the potential of this new concept for zero power remote sensing, two transducers have been fabricated for eye motion detection. One intended to monitor the Orbicularis Oculi (O.O) muscle beneath the eye's skin, and the other was a proof of concept for eyelid motion sensing. The accurate detection of such small body motions was possible with the assistance of high input impedance and high gain electronics. The O.O motion transducer was integrated into a portable prototype of an eye-movement based HMI for hands-free PC cursor control to support patients with limb disabilities, for easy interaction with the computer. The reported system differs from the one presented in Ref. [54] because it is not based on the standard TENG contact mode configuration, but instead combines the self-power properties of triboelectric devices with the near-field transmission of signals due to non-contact electrostatic induction. The system allows hands-free navigation on the web, to provide a true inclusion in the society and technology of handicapped patients without a third person intermediary. Finally, other applications using the O.O sensor such as hands-free remote car control, drone control, and driver fatigue monitoring, are also described and tested in this report.

2. Theory and calculations for voltage and efficiency of NEDTS for sensing and energy harvesting

Essentially, electrical induction theory states that a charge point induces an electric field \vec{E} in space as in Fig. 1a. In Fig. 1a the charged surface S , that lies in the 3-D space with orthogonal axis x, y , and z , generates an electric field \vec{E} in any point R' with coordinates x', y', z' . \vec{E} is quantified using the integral formula in Eq. (1), where R is any vector whose endpoint is in the surface S that lies in the 3-D space [62].

$$\vec{E} = \frac{1}{4\pi\epsilon_0} \iint_S \frac{\rho(\vec{R} - \vec{R}')}{|\vec{R} - \vec{R}'|^3} ds \quad (1)$$

When two surfaces contact each other as portrayed in Fig. 1b, the triboelectric effect makes the elements charge oppositely. When the surfaces move, the summation of the electric fields produced by each material is different from the null value, creating a resultant \vec{E} . If there is a metal plate in the space, the electric charges inside the equipotential conductor rearrange, creating an opposing electric field [63]. Eq. (2) presents the generated charge Q due to the electric field \vec{E} , on the lower face of the metallic surface with an area vector \vec{A} in the x, y, z space.

$$Q = -\epsilon_0 \oint_A \vec{E} \cdot d\vec{A} \quad (2)$$

This electric field reorganizes the charges in the metallic plate depending on the dielectric's motion and distance. Thus, if a load is connected to the electrode (metallic plate), current flows through it and a voltage value can be measured on the terminals of the load.

As standard, TENG devices combine the triboelectric effect and contact electrostatic induction, since the dielectric element is generally attached to the conductive electrode [10]. In contrast, in this project, the well-known “Contact Separation Mode” (CSM) configuration (Fig. 1c) is extended to a new topology named Non-attached Electrode-Dielectric Triboelectric Sensor (NEDTS) where the electrode is not coated on top of the dielectric (Fig. 1d) similar to the freestanding TENG in Ref. [25,59]. In Fig. 1d, the electrodes are separated from the insulator materials by distances $g_1(t)$ and $g_2(t)$. After contact, the two dielectric elements' surfaces acquire an opposing electric charge which is expressed as surface charge densities $+\sigma$ and $-\sigma$. If the theoretical analysis is done as in Ref. [64], the assumption that the area of the dielectrics surfaces S in Fig. 1d is larger than $g_1(t)$ and $g_2(t)$, leads to Eq. (3). The detailed process for the derivation of Eq. (3–5) is explained in the description of Fig. S1 in supporting information.

$$V = -\frac{Q}{S\epsilon_0} (d_0 + g_1(t) + g_2(t) + x(t)) + \frac{\sigma x(t)}{\epsilon_0} \quad (3)$$

In Eq. (3), $d_0 = d_1/\epsilon_1 + d_2/\epsilon_2$ and capacitances of gaps g_1 and g_2 sum up in a series, reducing the short circuit current and the overall power generation potential. To clarify the last statement, let us define the maximum value of the separation gap $x(t)$ as x_{max} . If it is assumed that d_0 is small compared to x_{max} , and the maximum values of the upper gap g_{1max} and lower gap g_{2max} are $\alpha x_{max}/2$ and $\beta x_{max}/2$ respectively, with α and β being distance ratios, the maximum charge due to short-circuit condition (when $V = 0$) becomes (see description of Figs. S1b–d in supporting information):

$$Q_{sc} = \frac{S\sigma x_{max}}{\frac{(\alpha+\beta)x_{max}}{2}} = \frac{S\sigma}{2} \frac{(\alpha+\beta)}{2} \quad (4)$$

In this case, charge transfer efficiency, which is the maximum short-circuit charge divided by the charge generated by friction which is σS (where σ is the surface charge density and S is the surface area of the dielectric layers) [29], becomes:

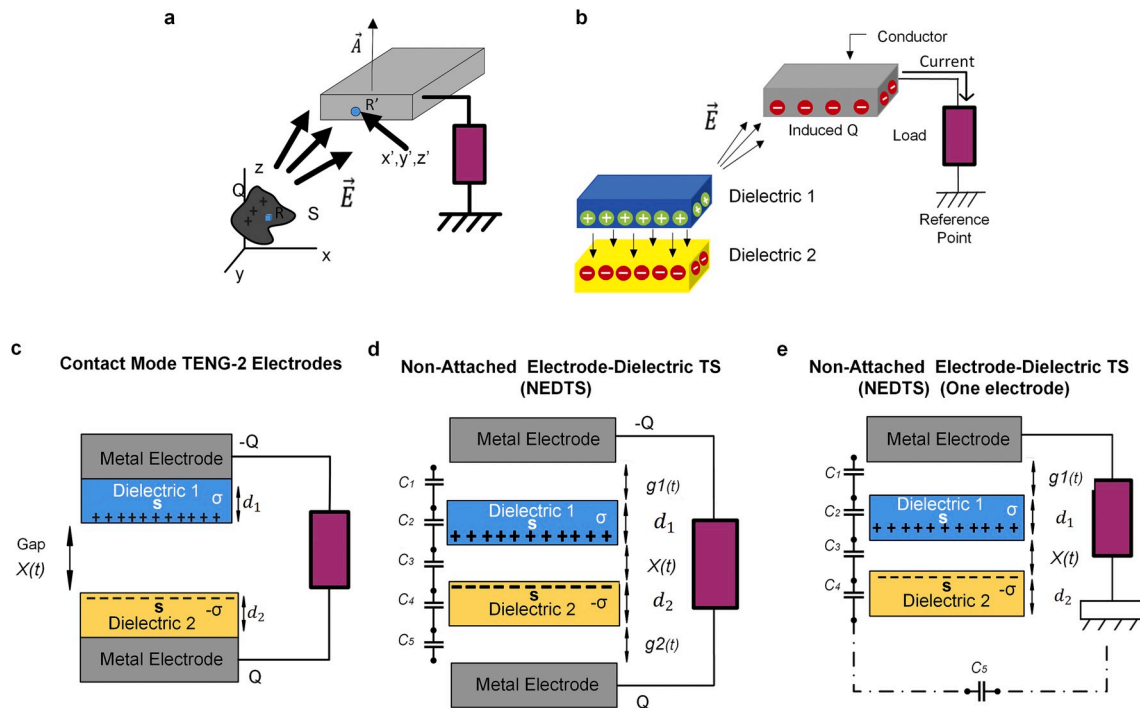


Fig. 1. Overview of the combined triboelectric effect and non-contact electrostatic induction. (a) Electrostatic induction due to a charged surface. (b) General topology of NEDTS for short-range remote sensing. (c) CSM Triboelectric Nanogenerator, where metal electrodes are coated to the dielectric materials. (d) Extended CSM TENG when a separation distance exists between the electrodes and the dielectrics. The new configuration is called NEDTS with two electrodes (e) NEDTS in single-electrode mode.

$$\eta = \frac{Q_{sc}}{S\sigma} = \frac{1}{\frac{\alpha}{2} + \frac{\beta}{2}} \quad (5)$$

For the simple CSM configuration, the charge transfer is ideally close to one [29]. Instead, for the arrangement presented in Fig. 1d the efficiency greatly differs from the unity value and is inversely proportional to the ratio of the maximum values of the gaps, because of $\alpha/2 = g_{1max}/x_{max}$ and $\beta/2 = g_{2max}/x_{max}$. In contrast, for Eq. (3) the open-circuit voltage value when $Q = 0$ is $\sigma x(t)/\epsilon_0$, which, with the assumptions made, proves that open-circuit voltage is proportional to the motion's dynamic. In practice is expected for this voltage to decay with distance [60] but still will be proportional to motion.

Likewise, the non-attached electrode-dielectric topology can also be applied as a single electrode TENG configuration as in Fig. 1e. In that case, the short circuit charge is shown in the explanation of Fig. S2a of supporting information and is inversely dependent on the ratio C_3/C_5 . Since C_5 is very low (could be neglected), the value for efficiency in Eq. (S33) under Fig. S2 in supporting information becomes even lower than the efficiency value for the configuration with two electrodes. Nevertheless, the open voltage value in Eq. (S34) (Fig. S2a, supporting information) can be significant for measurement purposes. Furthermore, if the last configuration is modified in such a way that the TENG is placed on the skin, a topology similar to the one shown in Fig. S2b is obtained. For that case, the short circuit current and charge transfer efficiency are also inversely dependent on the separation distance and the ratio between the capacitance of the gap between the dielectric and the capacitance of the human skin as denoted in Eq. (S35), (Fig. S2b, supporting information).

3. Results and discussion

3.1. Characterization of the NEDTS topology

Some experiments were performed to assess the voltage output from the NEDTS configuration. Fig. 2 presents the experimental setup, and the

results, due to the interaction between the human skin, the silicone-based material Ecoflex™, and a conductive polymer PEDOT: PSS-based film [13].

Fig. 2a presents the results when the materials under motion are the finger and the Ecoflex™. The metallic plate in Fig. 2a (i) is made from aluminium (Al) and is separated by distance g_{max} . Under two different maximum separation widths for g_{max} (3.3 cm and 5.3 cm), and a maximum gap distance for $x(t)$ of 1.7 cm, the results for voltage are presented in Fig. 2a (ii). In this case, for a load with an input impedance of 1 GΩ, the higher the distance, the lesser the voltage amplitude. Next, Fig. 2b (i) shows the setup used to assess the effect of Ecoflex™ and the arm skin when the maximum separation of $x(t)$ is 1 cm, and the two separation distances for g_{max} are 2 cm and 4 cm. The structure used to set the height of the conductive plate is presented in item (ii) (Fig. 2b). In Fig. 2b (iii), The Ecoflex™ is attached to the paperboard handler to produce the tapping motion (Fig. S3 of Supporting information). Fig. 2b (iv) demonstrates that, although voltage induction gets lower when the gap between dielectric and electrode increases, a measurable voltage value exists and is proportional to motion. In Fig. 2c (i), the triboelectric effect is tested between a finger and Ecoflex™ for horizontal gaps of 1.5 cm, 5 cm, and 7 cm. The results again show how voltage reduces when horizontal distance increases (Video S1 of Supporting information). The voltage signals are similar in amplitude to the results in Fig. 2a, and higher than the outcome from the experiment of Fig. 2b. Finally, Fig. 2d shows the output when the materials under motion are Ecoflex™ and a PEDOT: PSS-based thin film. The purpose of this final test (Fig. 2d) is to observe the waveform characteristics due to pressing and releasing actions at different speeds. As illustrated, the separation distance x between ECOFLEX™ and PEDOT:PSS-based film is about 1 cm and the distance between PEDOT:PSS-based film and the metal electrode is about 2 cm. Fig. 2d (iv), illustrates that the output signal for two different touch rates (1 Hz and 4 Hz) is less than 1V for a load resistance of 1 GΩ.

Supplementary video related to this article can be found at <https://doi.org/10.1016/j.nanoen.2020.104675>

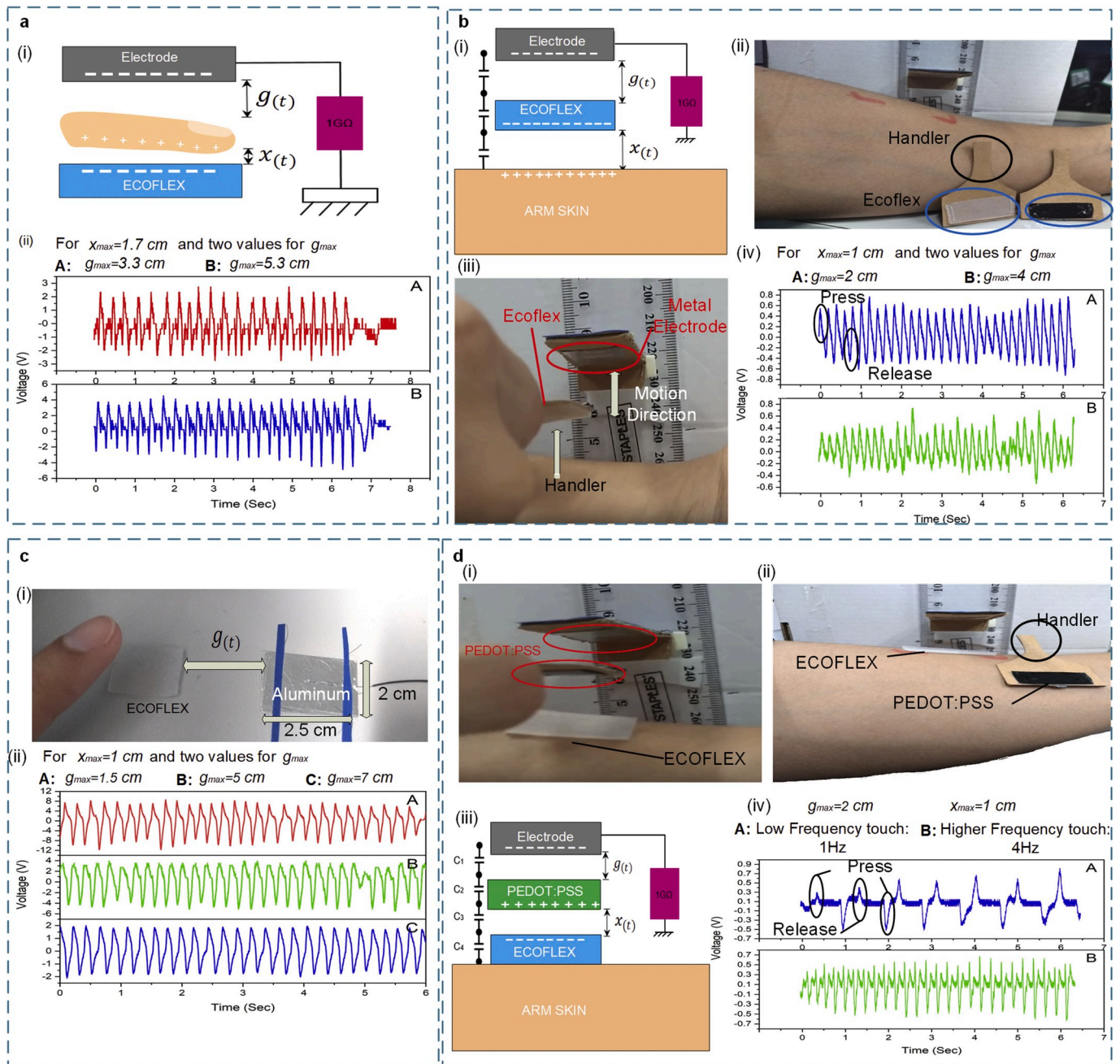


Fig. 2. Voltage results from preliminary experiments for NEDTS. (a) Finger tapping test. (i) The finger moves up and down with a maximum gap of 1.7 cm. (ii) Results using different heights for the metallic electrode. (b) Test of the triboelectric interaction of arm skin and Ecoflex™, (i) The flexible material moves up and down from the arm. (ii) Setup used for the experiment and handler device. (iii) Test Using Ecoflex™ mounted in the handler device. (iv) Results for two different vertical gaps. (c) Test of the interaction between finger and Ecoflex™ for a horizontal gap. (i) Three separation gaps are tested. (ii) Results for each horizontal gap. (d) Triboelectric interaction test for different touch rates, using PEDOT:PSS-based film (i) Setup used for the experiment. (ii) PEDOT:PSS film touches the Ecoflex™ at different frequencies. (iii) The Ecoflex™ lies on the skin. The metallic plate is separated with a maximum distance of 2 cm. (iv) Results for two different touch rates.

It is observed from the experiments that the triboelectric effect enhances the dynamic of the charge induction, helping the dielectrics (or skin) to work as better “charge inducing sources”. When the separation between dielectric and electrode changes, the value of the electric field also changes, inducing a non-constant voltage on the metallic plate. Even though the experiments demonstrate that voltage amplitude decreases when the gap increases, a voltage proportional to motion is still detected with enough amplitude for its applications as a TENG-based sensor.

Finally, when the non-attached mode between dielectric and electrode is used for energy harvesting, the usual separation space is set in

the order of millimeters [59,60]. Whereas in this project the topology demonstrates great potential for self-powered near-field remote wearable sensing in the order of centimeters. This result is significant for the design of wearable assistive devices, as it is gonna be explained in section 3.2.

3.2. Orbicularis Oculi's sensor design and characterization

Based on the results discussed above, an eye motion sensor aimed to monitor the eye muscle is designed. The sensor intends to measure the Orbicularis Oculi muscle motion to detect the eye blink. The O.O

muscle's primary functions are to close the eyelid and assist tear drainage and is found in the concentric surface around the eye as portrayed in Fig. 3a [65,66]. Hence, the O.O muscle is sensed by placing a NEDTS directly on one side of the eye (Fig. 3a).

The TENG sensor in Fig. 3b is adapted from the work in Ref. [13]. The PEDOT:PSS is attached to the Ecoflex™ layer by using a textile thread and the sensor dimensions are 1.5 cm × 0.6 cm × 2 mm. When placed on the lateral skin tissue of the eye, the O.O muscle, which is underneath the sensor, triggers an output when it is voluntarily or involuntarily moved. When the muscle moves, the two layers rub each other, transferring opposite charges. Also, an electrode plate is attached to the lateral temple of the eyeglasses separated approximately 1.5 cm away from the NEDTS (Fig. 3c (i)). Depending on the position and the

size of the sensor, the muscle contraction or relaxation causes the PEDOT:PSS film and the ECOFLEX™ to touch, so the charge is induced in the metal. The position of the sensor over the muscle is essential since a place that shows evident muscle contraction and relaxation should be used. An optimum position is found when a contraction of the O.O muscle stretches the sensor, so the PEDOT:PSS and the Ecoflex™ can make contact. For that case, the muscle relaxation separates the polymer layers.

Due to the small displacement nature of the eye muscle, the signal coming from a triboelectric sensor is expected to have a lower amplitude than the output values in Fig. 2. Consequently, a conditioning circuit is designed to amplify the voltage from such small motions. The circuit in Fig. S4 possesses a high input impedance stage, a high gain amplifier

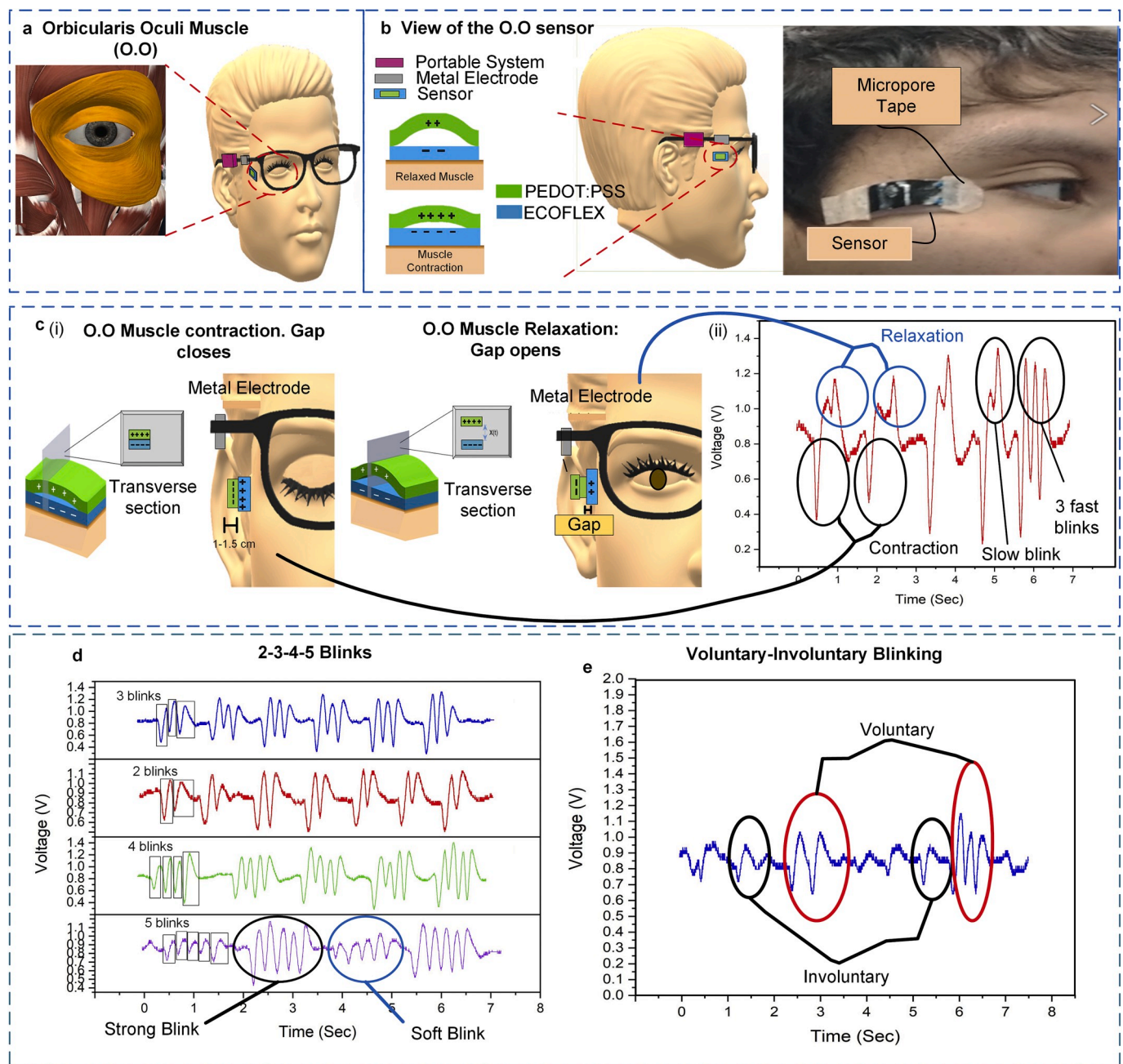


Fig. 3. Eye motion sensor design, placement, and results. (a) Orbicularis Oculi Muscle surrounds the surface beneath the eye. (b) Sensor overview, and placement. (c) (i) When the eye is closed, the muscle contracts and the sensor layers are stretched. When the eye is opened again, the muscle relaxes as well as the sensor layers. The transverse section is displayed. (ii) Contraction and relaxation signals. Fast and slow blink. (d) Output signal from two, three, four, and five (soft and strong) consecutive blinks. (e) Voluntary and involuntary flickers.

stage, and a notch filter stage to avoid 50 Hz line interference. The input stage has an impedance of approximately 10 MΩ, since a higher impedance could add more thermal noise to the signal. The amplifier stage has a gain of about 220 V/V and each stage has a passive low pass filter to increase the order of rejection of high-frequency noise. There is also a DC offset stage, so the voltage signals swing up and down with a mean value of 1V. The signal in the final stage swings from 0V to 2V, which can be detected by a low power microcontroller as the MSP430G2553 from TI. The circuit is sensitive to the electrostatic induction and not to the change of capacitance between the triboelectric layers close to the temple of the eyeglasses. Since the circuit can pick up electrostatic interference that comes from moving electrified objects, the electronic possesses a low pass filter to reject unwanted high-frequency signals from electrostatic noise. Moreover, there is a high pass filter in the final stage (capacitor and resistor network at the input of the final amplifier) that helps to reject low-frequency signals from slow motions of the human body (especially the head), which could be charged depending on the environment.

After analog amplification and noise filtering, Fig. 3c (ii) portrays the difference in contraction and relaxation motion when the eye flicker is slow. Contraction, after the eye closing, produces a negative voltage, while relaxation produces two positive peaks that are unable to be separately identified in faster motions (The identification of this peaks for slow blinks will be important for eye fatigue monitoring application explained in section 3.5). Fig. 3d illustrates the output after blinking two, three, four, and five times consecutively. Each blink is made by a negative and a positive peak that comes from the contraction and relaxation of the O.O muscle. As observed, the peak to peak voltage for each blink is about the same value in a range of 300 mV–600 mV. The plots show that the amplitude signal for the voluntary flicker is

approximately the same in all cases and does not decay in a short time. The purple signal in the same subfigure shows the response for five blinks when the closing-opening motion of the eye is soft or strong. In that case, the voltage signal is different for the two conditions. For a soft blink, the maximum value is 400 mV, while a tight flicker is about 600 mV. Finally, Fig. 3e displays the signals for voluntary and involuntary movement together. In this case, both outputs differ in the voltage amplitude again, which is expected. The voluntary action of closing the eyelid is governed by the orbital portion of the O.O muscle, and the soft motion is controlled by the palpebral portion. The palpebral portion closes the eye gently (involuntary), so the motion is expected to be slight compared to the contraction of the orbital part, which closes the eyelids tightly [66]. The results show that some low-frequency noise is observed due to the high input resistance and high amplification in the conditioning stage, but the signal is not significantly affected by it. Furthermore, although it is not necessary, a conductive electrode of any shape or size can be connected anywhere in the skin to connect the body to the circuit reference point (ground connection) offering more stability against low-frequency noise and body motion.

3.3. Cursor control application based on NEDTS

By using the NEDTS configuration for eye monitoring, an application for cursor control is developed. From the two previous devices, the O.O motion sensor was chosen due to its higher voltage and better comfortability. The presented development aims to help people with disabilities to have access to web services and computers using the designed O.O NEDTS.

First, the circuit in Fig. S4 is just part of a complete portable measurement system intended for micromotion monitoring. The device in

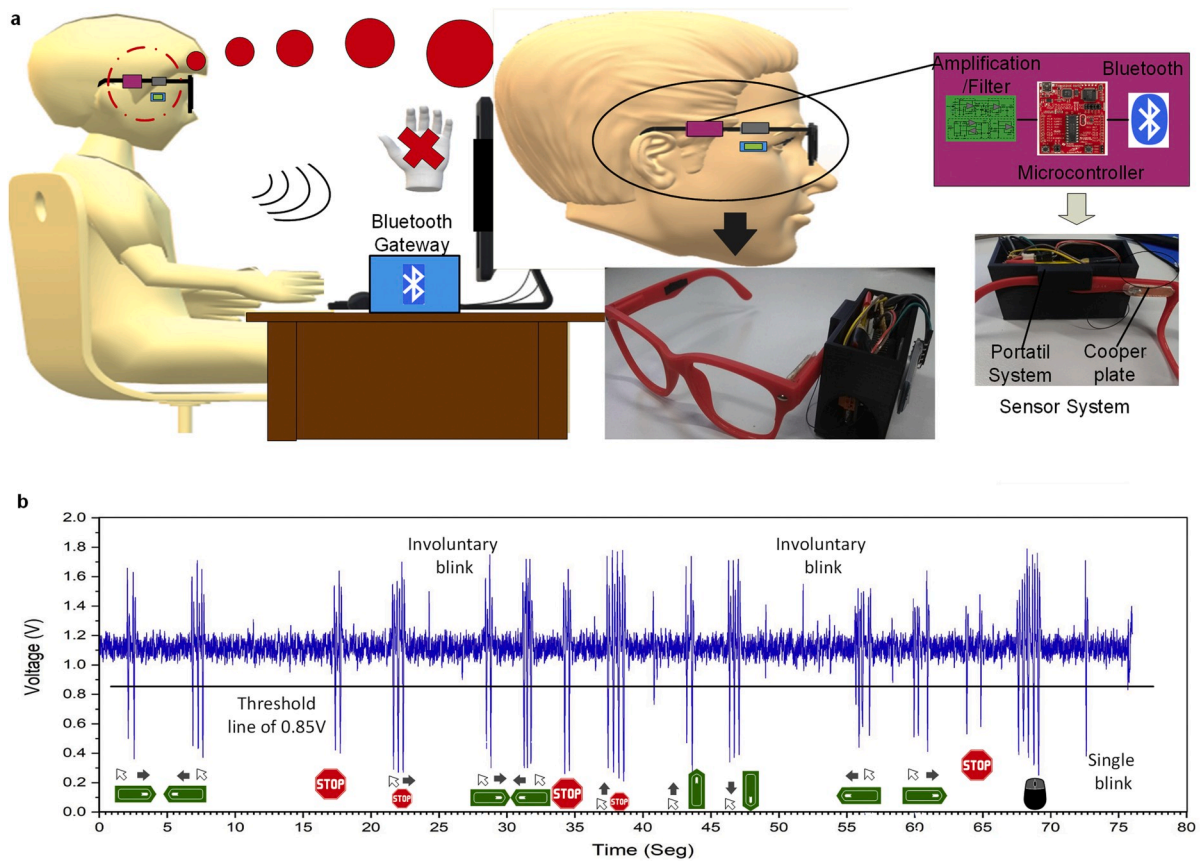


Fig. 4. Complete HMI system for cursor control. (a) Sensor motion is amplified and posteriorly digitalized by the microcontroller. The controller sends the information wirelessly through Bluetooth for post-processing. (b) Sample of the signal read by the python code when controlling the cursor. The control sequence for the cursor motion is presented until a click action is performed.

Fig. 4a works with a 3.3 V supply and a low power MSP430 microcontroller (MCU), which reads the output voltage using an ADC. The information is then transmitted using a Bluetooth transceiver connected to the MCU. A second Bluetooth gateway receives the signal and transfers the information to the computer for post-processing.

Second, the software, coded in python, allows controlling the cursor and the left click so the user can navigate on the internet. In Fig. S5 on supporting information, it is shown the flowchart of the software instructions depending on the number of flickers. The cursor always has initial position and direction settings, which can be in the x-axis (positive or negative) or the y-axis (positive or negative). If the user blinks two times, the cursor moves in the initial direction being x or y. If the person blinks twice again, the cursor stops. When the person flickers three times in a row, the axis direction setting is changed 180°. If the

person blinks four times, then the axis direction changes 90°. Finally, five blinks perform the left click action. To avoid any mistake between voluntary and involuntary blink, “one blink action” is not considered a significant input for the software. If desired, the code can be modified further, adding more functionalities for a higher number of blinks as depicted in Fig. S5, demonstrating the versatility of the proposal.

The signal amplitude and the number of consecutive blinks were recognized by setting a voltage threshold in the code for the negative peaks as in Fig. 4b. As observed in Figs. 3 and 4a, each blink shape is made by at least a negative peak followed by a positive peak. Although the lower threshold is the critical base to recognize a blink, the software decides also by observing the positive voltage peaks of the signal that follows the down peak of the blink. As observed in Fig. 3, each blink shape is made by at least a negative peak followed by a positive peak.

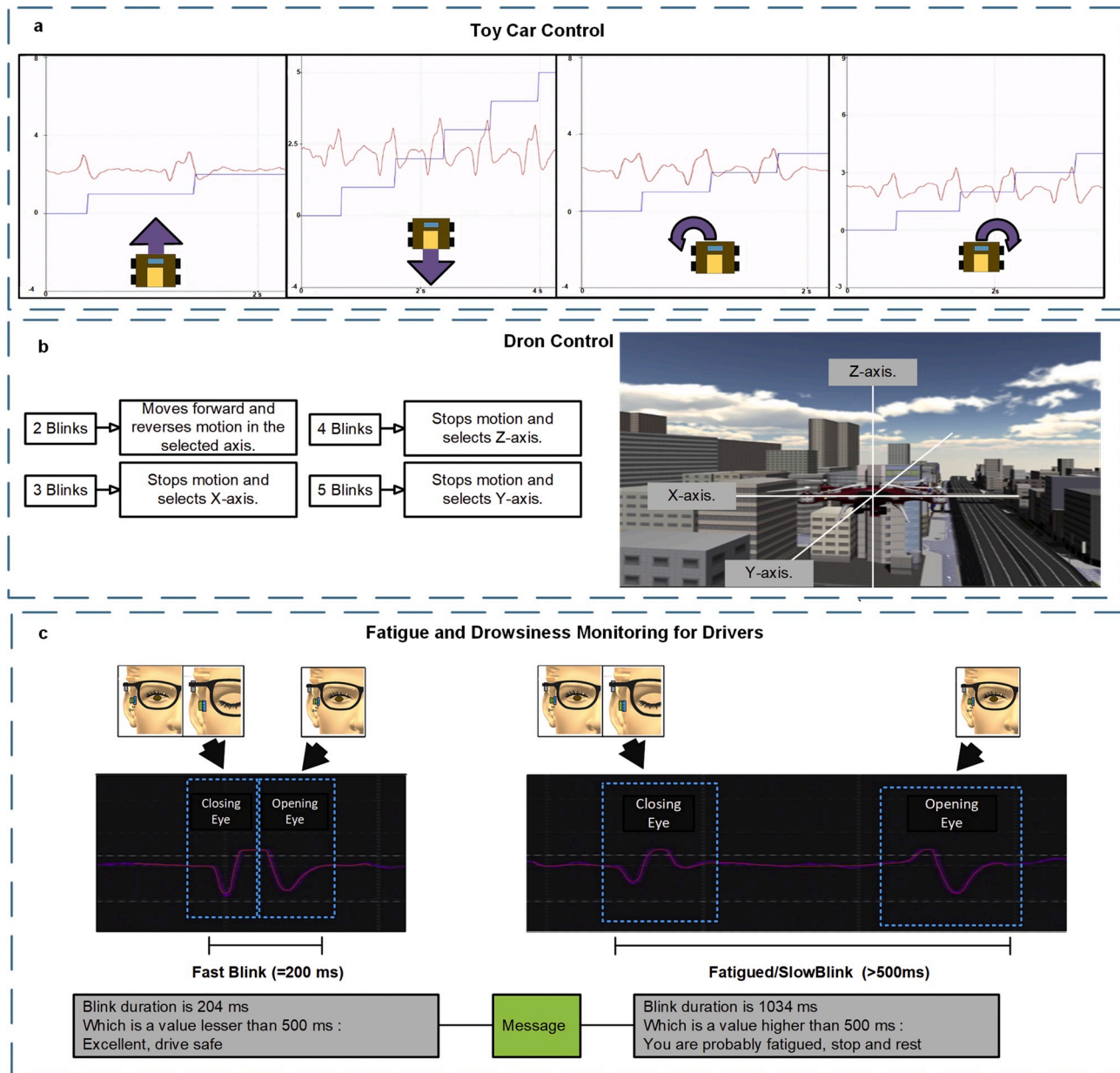


Fig. 5. The Orbicularis Oculi motion sensor used in applications as car control, drone control and fatigue monitoring for drivers. (a) Different number of blinks select the direction of the remote toy car. There is no stop instruction since the car is programmed to stop 2 s after a forward or backward instruction. (b) The virtual drone control follows an algorithm similar to the one used for hands-free cursor control. (c) The system is also used for fatigue monitoring. A closing eye movement generates a negative peak followed by a smaller positive peak. An opening eye movement results in a positive peak followed by a negative peak. That way a closed eye is differentiated from an opened eye, as well a fast blink is distinguished from a slow blink, which can indicate driver fatigue (the signal is repainted in red for illustration purposes, See Fig. S7 in Supporting information).

Since involuntary blink amplitude is less than the threshold, no instruction is executed. Moreover, a random signal shape different from the eye blink characteristic signal, which results from the electrostatic noise, can be neglected by the software. In Fig. 4b is observed the time and the number of blinks required to move the cursor until the execution of a click action. It takes around 70 s for the correct positioning of the cursor in a toggle button of a web page. It is good to remember that the direction setting can change 180° or 90° no matter the cursor motion status (moving or standing by). In Fig. 4b, the green signal indicates that the cursor starts motion in the direction of the grey arrow. On the other hand, the red stop signal indicates that the cursor is not moving even if the direction setting changes due to a specific blink count. The big “stop signal” in the image, below two consecutive blinks, indicates that the cursor is standing by and no axis change has been performed. Finally, some problems with low-frequency noise were corrected by adjusting the threshold and position of the sensor. For the performed test, the Signal-to-Noise ratio (SNR) of the blink signal compared to the background noise is about 13 dB, which as demonstrated, allows the recognition of the blink over the noise.

Video S2 of Supporting information shows the working principle of the system and the placement of the sensor on top of the O.O muscle. By the above cursor control method, the new concept of a full-screen navigation system based on eye motion is possible for people with upper limb disabilities. Video S2–S3 of supporting information, demonstrate the functionality of the device when surfing the Internet.

Supplementary video related to this article can be found at <https://doi.org/10.1016/j.nanoen.2020.104675>

3.4. Remote car control, drone control, and driver fatigue monitoring based on NEDTS

Other demonstrations have been performed to validate the high range of applications of this new O.O triboelectric sensor. In Fig. 5a–b and video S4–S5 of Supporting information, the implementation of this sensor for virtual drone control and remote car control is demonstrated. Following a similar logic as in the cursor control application, the direction of drone and car is selected by the number of blinks (Note 7 on supporting information). Finally, the proposed sensor topology can also be used for eye fatigue monitoring applications. As observed in Fig. 3c (ii), one normal blink produces a signal which has a positive and negative peak and quickly goes back to zero. However, when the eye flicker is slow, the negative and positive peaks are separated in time. This duration time can give information or warn about eye fatigue or drowsiness when a person is driving [66]. Consequently, this information can be used to set up an alarm for the driver to advise him/her to stop and rest. Thus, triboelectric sensors could also be implemented for accident prevention. This last function is illustrated in Fig. 5c and in video S6 of Supporting information where it is compared the blink motion for a person with adequate driving awareness with the same person emulating sleepiness or fatigue. For this particular case, a different and more sensitive circuit was assembled to recognize involuntary slow motions (Fig. S6 of Supporting information). The closing eye and opening eye signals can be differentiated using the newly designed circuit based on a charge amplifier input stage. The time duration of one normal blink was observed to be about 200–300 ms, which is coherent with literature statements of 300–400 ms [67,68] for blink duration. In contrast, for a slow blink indicating fatigue or drowsiness, it takes more than 400 ms. Based on the above, the screen in video S7 of Supporting information shows a message when the person emulates tiredness (blink duration more than 500 ms), advising him/her to stop driving to take a rest (These messages are also portrayed in Fig. 5c). The system also recognizes when the person has kept his/her eyes closed for more than 1s. At this point, the person probably has fallen asleep, and a different message is displayed in video S6 emulating a required alarm action.

Supplementary video related to this article can be found at <https://doi.org/10.1016/j.nanoen.2020.104675>

[://doi.org/10.1016/j.nanoen.2020.104675](https://doi.org/10.1016/j.nanoen.2020.104675)

3.5. Demonstration of NEDTS configuration with a non-parallel arrangement between the electrode and the triboelectric layers

Finally, in order to demonstrate the versatility of the new NEDTS arrangement, a second sensor was developed based on the remote sensing feature. This particular sensor is a thin flexible PDMS film shaped to be placed on top of the eyelid (Fig. 6a). The working principle is based on the triboelectric effect between the polymer and the eyelid skin. When the eye opens and closes, the eyelid folds and allows contact between the PDMS patch and the epidermis below the eyebrow as illustrated in Fig. 6b. The eyelid folding motion charges the dielectric and consequently induces some charge in the electrode placed in the upper rim of the glass. Fig. 6c illustrates the results when the eye closes (press) and opens (release) voluntarily. Fig. 6d plots the output for one, two, three, four, and five consecutive blinks. Video S7 of Supporting information shows the placement and the output signal of this arrangement.

In contrast with the O.O sensor, which follows the configuration in Fig. 1c, where the dielectric layers are mostly parallel to the electrode, in Fig. 6b, the near field electrostatic induction is achieved even when the triboelectric interaction between skin and PDMS is not parallel to the electrode. Hence, this final test demonstrates that the NEDTS can be implemented by following the general structure in Fig. 1b where the tribo-layers are not necessarily parallel to the conductive electrode as in the horizontal distance test in Fig. 2d. Nevertheless, this particular sensor is limited by the biological structure of the human body. People have different eyelid shapes and sizes, which means that this configuration should consider these variations for optimized wearable design. Finally Fig. S8 in supporting information provides more insights for this sensor.

4. Discussion

So far, most of the TENGs used in the existent approaches as transducers require the electrode and the dielectric to be attached. Those electrodes connect to wires which are posteriorly connected to non-portable devices such as electrometers for sensor characterization and testing.

In this work, a new concept of TSs was investigated for small distance remote sensing, based on free-standing configuration, leading to new wearable design approaches. The clear advantage of the new topology over other schemes is the non-contact electrostatic induction effect, which eliminates the need to coat a conductive layer followed by a large size wire, on top of the sensor. Non-lead configurations with the proposed topology for on-body applications are preferable to ensure people's comfort when using wearable devices.

The hardware designed for signal amplification can be integrated into any triboelectric-based system due to its high input impedance and its portability features. The application of the new concept for NEDTS configuration in a hands-free HMI interface for cursor control demonstrates that the sensor and the designed hardware can be used together in the future of the biomedical field, helping people with disabilities. Additionally, since the electronic circuit is very sensitive, it can be connected to other TENGs intended to track specific muscle micro-motions, like arm muscles to assess different diseases such as Parkinson's and epilepsy.

As part of the discussion, it is essential to mention some limitations and suggestions. Even with the O.O muscle surrounding the eye, position selection poses a condition that impacts the signal amplitude significantly. Once a satisfactory place is found, then the signal can be read and recognized by the microcontroller. Sweat also causes the sensor to detach from the skin and it needs to be re-attached to the O.O muscle. For further research, the sensor-to-skin attachment method needs to be improved to prevent patient discomfort and performance loss due to

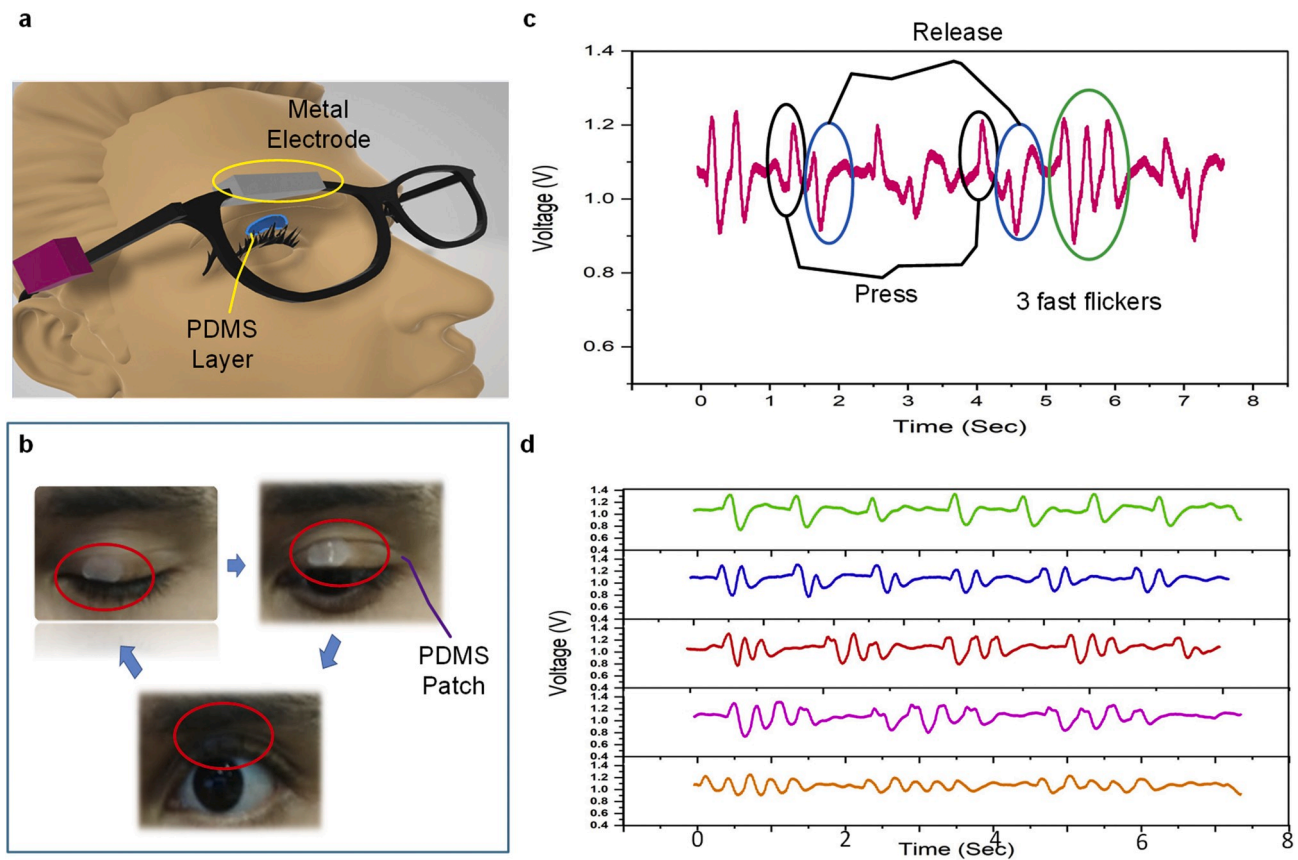


Fig. 6. Output signals for the PDMS-based eyelid sensor. (a) 3-D view of the eyelid motion sensor system. (b) Output signal from eyelid motion. (c) PDMS-SKIN contact sequence due to eyelid motion. (d) Output signal for one, two, three, four, and five consecutive blinks. (e) Output for voluntary and involuntary blinks.

sweat and head motion for long-term implementation.

Regarding the eyelid sensor, it can be initially analyzed as a proof of concept, which demonstrates that, with the right electronic stages, a small motion can be detected even if the conductive plate is not placed parallel to the triboelectric layers. The limitation of this configuration is mainly due to people's different eyelid shapes and sizes, making this configuration hard to implement with accuracy in a broad group of people.

Nevertheless, the applied O.O sensor and the eyelid sensor demonstration opens the path for the fabrication of innovative and creative TENG shapes using different materials, and motions, to monitor specific parts of the body. What is more, the NEDTS configuration can lead to the creation of implantable sensors that send the motion signal of heart or inner organs, through near field electrostatic induction without connecting any hardware inside the body. The possibilities of application are far-reaching in the field of micromotion monitoring in inner and outer tissues of the body.

5. Conclusion

In this paper, a new TENG configuration has been implemented for micromotion monitoring from the human body. By modifying the standard contact mode and free-standing configuration for TENGs we have developed a triboelectric/electrostatic coupled novel approach for low-range distance remote sensing of body micromotions. Such an approach lead to a new IoT wearable sensing concept for healthcare applications, demonstrated by the design of a portable eye motion tracker prototypes (O.O muscle sensor) integrated into an HMI system for the assistance of disabled people.

We demonstrated the successful use of the O.O sensor in an HMI prototype for hands-free cursor control due to small eye muscles. By

tracking the number of blinks, the cursor could move on the screen, allowing internet navigation without a mouse. Additionally, the proposed sensor proved itself useful in other applications, as hands-free remote drone and car control, as well as monitoring driver's fatigue. The sensor and the developed system were able to recognize the difference when a person simulated fatigue or sleepiness giving a screen alert. Moreover, the control software can be upgraded with other functionalities and optimized depending on the requirements of the patient, by adding more options according to a higher blink count or the time between different blink actions. On the other hand, despite its limitations, the eyelid sensor configuration demonstrated that the NEDTS configuration can provide motion information even if the conductive plate is not placed parallel to the triboelectric layers.

Since the materials used for the development of the sensor and system are cheap and easy to integrate, the sensor could be easily used in disabled people with low monetary resources to guarantee their access to novel technologies. Ultimately, this report endeavours to inspire more research in the development of novel, low cost, flexible and fully portable micromotion monitoring systems aimed to play a vital role in the inclusion in society and technology of people with physical disabilities.

6. Materials and methods

6.1. Fabrication of Ecoflex™ and PDMS layer

The fabrication process for the triboelectric layers is similar to the methods explained in Ref. [69]. The Ecoflex™ 00–30 is a silicone-based commercial product fabricated by Smooth-On. The material is a mixture 1:1 from components A and B. The mixture was cast in a mold and was exposed to ambient temperature for about 4–5 h until it is completely

cured. The material was then cut and shaped according to the desired dimensions. The PDMS is a mixture 10:1 of two liquid compounds from Dow Corning. The mixture was left in a glass petri dish and heated. After some hours, the material was finally cured and shaped in order to be placed on top of the eyelid. For this project, no patterned mold was used in the manufacturing of the silicon-based triboelectric sensors. Probably, a patterned mold will allow more charge transfer in the surface of the triboelectric layers, increasing the voltage output and the sensitivity to small motions of the eye muscle.

6.2. Fabrication of PEDOT:PSS film

The PEDOT-based film was also used in Refs. [70]. PEDOT:PSS solution was added to 5 wt% DMSO, and it was then mixed with 20 wt% water-borne polyurethane WPU solution by vigorously stirring at room temperature for half an hour. The weight ratio of PEDOT:PSS to WPU was 1/19. The PEDOT:PSS/WPU blend films were prepared by drop-casting the dispersions in a glass Petri dish [70]. They were then dried at 70 °C in an oven for 12 h.

6.3. Electronic circuit and setup for the characterization of the triboelectric sensor

For the characterization stage, the measurement circuit is illustrated in Fig. S9 of Supporting information. For the acquisition of the signal, the digital oscilloscope ADALM2000 was connected to the designed measurement circuit which has an input impedance of 1GΩ. The ADALM2000 board is connected to the computer, and the signal is visualized using the Analog Devices software SCOPY which also allows the storage of the signal in a CVS file. The circuit has a voltage divider with a 20 to 1 ratio, which means that the output should be multiplied 20 times to obtain the original value. It also possesses a low pass filter and a 50 Hz notch-filter to reject non-desirable frequency components.

6.4. Fabrication of the eye muscle and eyelid motion sensors

The PEDOT:PSS based film was bonded to the Ecoflex™ layer by using a textile thread. In the center of the sensor, a space of about 0.5 cm was left between the silicon-based layer and the PEDOT:PSS-based layer. The sensor is placed in the muscle under measurement (the Orbicularis Oculi [O.O] muscle). The placement should guarantee that a muscle contraction should make the two layers touch each other, and a muscle relaxation should allow the separation of the layers. The eyelid sensor is just a thin PDMS layer shaped like an oval so it can be placed carefully on top of the tissue.

6.5. Assembling of the portable cursor control system and fatigue monitoring system

The circuit in Fig. S4 was fabricated into a printed circuit board PCB using SMD components. The circuit was powered by a LIPO battery with a voltage of 4.3/3.7V. The voltage was regulated by using the board MIKROE-3035 and L78L33ACZ to provide a supply voltage of 3.3 V. The signal was read using the ADC of the low power MSP430G2553 microcontroller IC. The wireless data transmission was achieved using the BLE module HC-05. All the modules and components were placed in a 3d-printed enclosure designed to be placed in the plastic glass temple. The metallic plate used is a 2.5 cm × 1 cm rectangle made of RF4 which was coated on top with a copper layer (commercially available in any electronics store). These are the same materials used for the standard fabrication of Printed Circuit Boards (PCBs). The plate was stuck to the glass temple using double-sided tape. The system described above was used in the HMI prototype for computer cursor control, remote drone and car control by voluntary blinks. In the 3D printed enclosure, a rectangle of aluminium tape was attached, so it touched the human skin when the glasses are worn. The aluminium connects the skin to a ground

reference, giving more stability to the circuit for the rejection of low-frequency noise. It is worth to mention that a second prototype which integrated all the components of the system (amplifier, filtering stages, microcontroller and Bluetooth module (Nrf52840 from Nordic) in a single PCB was fabricated and tested. The advantage of the second prototype was the reduction in size and the easy migration to a flexible PCB version as portrayed in Fig. S10 of supporting information.

In the case of the fatigue monitoring system, the primary purpose is to monitor involuntary blinks, thus a more sensitive circuit was designed. The circuit in Fig. S6 worked as a charge amplifier with high gain, filtering frequencies above 10 Hz, especially 50 HZ, and the corresponding harmonic components. This circuit was not integrated into a portable system as the first conditioning circuit was. On the contrary, the circuit was assembled on a standard breadboard. The input was connected to the metallic plate using a thin flexible copper cable. The length of the cable is critical because of the circuit's sensitivity. External mobile charged objects like the human body can generate low-frequency noise which increases with the length of the cable. The action of connecting the ground of the circuit with any part of the skin, even though it is not necessary, reduces the noise and allows more stability in the output signal. In this case, the circuit is powered by a dual supply of +5V and -5V using the measurement board ADALM2000 from Analog Devices Inc.

6.6. Code development and software

The algorithm for the eye cursor control was written in Python. The program for remote car control was written using the Arduino Integrated Development Environment. Finally, the virtual drone simulation was done in real-time development platform Unity 3D.

Declaration of competing interest

The authors declare that they have no known competing financial interests or personal relationships that could have appeared to influence the work reported in this paper.

CRediT authorship contribution statement

David Vera Anaya: Conceptualization, Methodology, Software, Investigation, Writing - original draft, Formal analysis, Visualization, Project administration. **Tianyi He:** Resources, Software, Writing - review & editing. **Chengkuo Lee:** Supervision, Funding acquisition, Writing - review & editing. **Mehmet R. Yuces:** Supervision, Project administration, Writing - review & editing, Funding acquisition.

Acknowledgments

This work was primarily supported by the Australian Research Council Future Fellowships Grant (FT130100430) and partly supported by the grant from the National Research Foundation: Competitive Research Project 'Peripheral Nerve Prostheses: A Paradigm Shift in Restoring Dexterous Limb Function' (NRF-CRP10-2012-01), and the grant from the HIFES Seed Funding: 'Hybrid Integration of Flexible Power Source and Pressure Sensors' (R-263-501-012-133).

Appendix A. Supplementary data

Supplementary data to this article can be found online at <https://doi.org/10.1016/j.nanoen.2020.104675>.

References

- [1] J. Kim, A.S. Campbell, B.E.-F. de Ávila, J. Wang, Wearable biosensors for healthcare monitoring, *Nat. Biotechnol.* 37 (2019) 389–406, <https://doi.org/10.1038/s41587-019-0045-y>.

- [2] M.M. Rodgers, V.M. Pai, R.S. Conroy, Recent advances in wearable sensors for health monitoring, *IEEE Sensor. J.* 15 (2015) 3119–3126, <https://doi.org/10.1109/JSEN.2014.2357257>.
- [3] S. Choi, H. Lee, R. Ghaffari, T. Hyeon, D.-H. Kim, Recent advances in flexible and stretchable bio-electronic devices integrated with nanomaterials, *Adv. Mater.* 28 (2016) 4203–4218, <https://doi.org/10.1002/adma.201504150>.
- [4] T.Q. Trung, N.-E. Lee, Flexible and stretchable physical sensor integrated platforms for wearable human-activity monitoring and personal healthcare, *Adv. Mater.* 28 (2016) 4338–4372, <https://doi.org/10.1002/adma.201504244>.
- [5] N. Mozaffari, J. Rezaazadeh, R. Farahbakhsh, S. Yazdani, K. Sandrasegaran, Practical Fall Detection Based on IoT Technologies: A Survey, *Internet of Things*, 2019, p. 100124, <https://doi.org/10.1016/j.iot.2019.100124>.
- [6] M. Haghi, K. Thurow, R. Stoll, Wearable devices in medical internet of things: scientific research and commercially available devices, *Healthc. Inform. Res.* 23 (2017) 4–15, <https://doi.org/10.4258/hir.2017.23.1.4>.
- [7] C. Qiu, F. Wu, Q. Shi, C. Lee, M.R. Yu, Sensors and control interface methods based on triboelectric nanogenerator in IoT applications, *IEEE Access* 7 (2019) 92745–92757, <https://doi.org/10.1109/ACCESS.2019.2927394>.
- [8] M.C. Domingo, An overview of the Internet of Things for people with disabilities, *J. Netw. Comput. Appl.* 35 (2012) 584–596, <https://doi.org/10.1016/j.jnca.2011.10.015>.
- [9] A. Ghorbel, N. Ben Amor, M. Jallouli, A survey on different human-machine interactions used for controlling an electric wheelchair, *Procedia Comput. Sci.* 159 (2019) 398–407, <https://doi.org/10.1016/J.PROCS.2019.09.194>.
- [10] X.S. Zhang, M. Han, B. Kim, J.F. Bao, J. Brugger, H. Zhang, All-in-one self-powered flexible microsystems based on triboelectric nanogenerators, *Nano Energy* 47 (2018) 410–426, <https://doi.org/10.1016/j.nanoen.2018.02.046>.
- [11] S. Jung, S. Hong, J. Kim, S. Lee, T. Hyeon, M. Lee, D.-H. Kim, Wearable fall detector using integrated sensors and energy devices, *Sci. Rep.* 5 (2015) 17081, <https://doi.org/10.1038/srep17081>.
- [12] X. Zhao, Z. Kang, Q. Liao, Z. Zhang, M. Ma, Q. Zhang, Y. Zhang, Ultralight, self-powered and self-adaptive motion sensor based on triboelectric nanogenerator for perceptual layer application in Internet of things, *Nano Energy* 48 (2018) 312–319, <https://doi.org/10.1016/J.NANOEN.2018.03.072>.
- [13] T. He, Z. Sun, Q. Shi, M. Zhu, D.V. Anaya, M. Xu, T. Chen, M.R. Yu, A.V.Y. Thean, C. Lee, Self-powered glove-based intuitive interface for diversified control applications in real/cyber space, *Nano Energy* 58 (2019) 641–651, <https://doi.org/10.1016/j.nanoen.2019.01.091>.
- [14] B. Dudem, A.R. Mule, H.R. Patnam, J.S. Yu, Wearable and durable triboelectric nanogenerators via polyaniline coated cotton textiles as a movement sensor and self-powered system, *Nano Energy* 55 (2019) 305–315, <https://doi.org/10.1016/j.nanoen.2018.10.074>.
- [15] H. Chen, L. Bai, T. Li, C. Zhao, J. Zhang, N. Zhang, G. Song, Q. Gan, Y. Xu, Wearable and robust triboelectric nanogenerator based on crumpled gold films, *Nano Energy* 46 (2018) 73–80, <https://doi.org/10.1016/J.NANOEN.2018.01.032>.
- [16] Y. Guo, X.S. Zhang, Y. Wang, W. Gong, Q. Zhang, H. Wang, J. Brugger, All-fiber hybrid piezoelectric-enhanced triboelectric nanogenerator for wearable gesture monitoring, *Nano Energy* 48 (2018) 152–160, <https://doi.org/10.1016/j.nanoen.2018.03.033>.
- [17] J. Xiong, P. Cui, X. Chen, J. Wang, K. Parida, M.-F. Lin, P.S. Lee, Skin-touch-actuated textile-based triboelectric nanogenerator with black phosphorus for durable biomechanical energy harvesting, *Nat. Commun.* 9 (2018) 4280, <https://doi.org/10.1038/s41467-018-06759-0>.
- [18] Z. Saadatnia, S.G. Mosanenzadeh, E. Esmailzadeh, H.E. Naguib, A high performance triboelectric nanogenerator using porous polyimide aerogel film, *Sci. Rep.* 9 (2019) 1370, <https://doi.org/10.1038/s41598-018-38121-1>.
- [19] K. Xia, Y. Chi, J. Fu, Z. Zhu, H. Zhang, C. Du, Z. Xu, A triboelectric nanogenerator based on cosmetic fixing powder for mechanical energy harvesting, *Microsyst. Nanoeng.* 5 (2019) 26, <https://doi.org/10.1038/s41378-019-0066-1>.
- [20] J. Zhong, Y. Zhang, Q. Zhong, Q. Hu, B. Hu, Z.L. Wang, J. Zhou, Fiber-based generator for wearable electronics and mobile medication, *ACS Nano* 8 (2014) 6273–6280, <https://doi.org/10.1021/nn501732z>.
- [21] F.R. Fan, Z.Q. Tian, Z. Lin Wang, Flexible triboelectric generator, *Nano Energy* 1 (2012) 328–334, <https://doi.org/10.1016/j.nanoen.2012.01.004>.
- [22] S. Wang, L. Lin, Z.L. Wang, Triboelectric nanogenerators as self-powered active sensors, *Nano Energy* 11 (2015) 436–462, <https://doi.org/10.1016/j.nanoen.2014.10.034>.
- [23] M.S. Rasel, P. Maharjan, M. Salauddin, M.T. Rahman, H.O. Cho, J.W. Kim, J. Y. Park, An impedance tunable and highly efficient triboelectric nanogenerator for large-scale, ultra-sensitive pressure sensing applications, *Nano Energy* 49 (2018) 603–613, <https://doi.org/10.1016/j.nanoen.2018.04.060>.
- [24] H. Zhang, Y. Yang, Y. Su, J. Chen, K. Adams, S. Lee, C. Hu, Z.L. Wang, Triboelectric nanogenerator for harvesting vibration energy in full space and as self-powered acceleration sensor, *Adv. Funct. Mater.* 24 (2014) 1401–1407, <https://doi.org/10.1002/adfm.201302453>.
- [25] H. Wang, Z. Xiang, P. Giorgia, X. Mu, Y. Yang, Z.L. Wang, C. Lee, Triboelectric liquid volume sensor for self-powered lab-on-chip applications, *Nano Energy* 23 (2016) 80–88, <https://doi.org/10.1016/j.nanoen.2016.02.054>.
- [26] W. Xu, M.-C. Wong, J. Hao, Strategies and progress on improving robustness and reliability of triboelectric nanogenerators, *Nano Energy* 55 (2019) 203–215, <https://doi.org/10.1016/J.NANOEN.2018.10.073>.
- [27] Q. Jing, Y. Xie, G. Zhu, R.P.S. Han, Z.L. Wang, Self-powered thin-film motion vector sensor, *Nat. Commun.* 6 (2015) 8031, <https://doi.org/10.1038/ncomms9031>.
- [28] M. Olsen, R. Zhang, J. Örtengren, H. Andersson, Y. Yang, H. Olin, Frequency and voltage response of a wind-driven fluttering triboelectric nanogenerator, *Sci. Rep.* 9 (2019) 5543, <https://doi.org/10.1038/s41598-019-42128-7>.
- [29] Z.L. Wang, L. Lin, J. Chen, S. Niu, Y. Zi, Triboelectric Nanogenerators, Springer International Publishing, Cham, 2016, <https://doi.org/10.1007/978-3-319-40039-6>.
- [30] Q. Zheng, H. Zhang, B. Shi, X. Xue, Z. Liu, Y. Jin, Y. Ma, Y. Zou, X. Wang, Z. An, W. Tang, W. Zhang, F. Yang, Y. Liu, X. Lang, Z. Xu, Z. Li, Z.L. Wang, *In vivo* self-powered wireless cardiac monitoring via implantable triboelectric nanogenerator, *ACS Nano* 10 (2016) 6510–6518, <https://doi.org/10.1021/acsnano.6b02693>.
- [31] X. Pu, H. Guo, Q. Tang, J. Chen, L. Feng, G. Liu, X. Wang, Y. Xi, C. Hu, Z.L. Wang, Rotation sensing and gesture control of a robot joint via triboelectric quantization sensor, *Nano Energy* 54 (2018) 453–460, <https://doi.org/10.1016/j.nanoen.2018.10.044>.
- [32] R. Zhang, M. Hummelgård, J. Örtengren, M. Olsen, H. Andersson, H. Olin, Interaction of the human body with triboelectric nanogenerators, *Nano Energy* 57 (2019) 279–292, <https://doi.org/10.1016/j.nanoen.2018.12.059>.
- [33] All-fiber hybrid piezoelectric-enhanced triboelectric nanogenerator for wearable gesture monitoring, *Nano Energy* 48 (2018) 152–160, <https://doi.org/10.1016/J.NANOEN.2018.03.033>.
- [34] Z. Wen, Y. Yang, N. Sun, G. Li, Y. Liu, C. Chen, J. Shi, L. Xie, H. Jiang, D. Bao, Q. Zhao, X. Sun, A Wrinkled Pedot, PSS film based stretchable and transparent triboelectric nanogenerator for wearable energy harvesters and active motion sensors, *Adv. Funct. Mater.* 28 (2018) 1803684, <https://doi.org/10.1002/adfm.201803684>.
- [35] Y. Zi, S. Niu, J. Wang, Z. Wen, W. Tang, L. Wang Zhong, ARTICLE Standards and figure-of-merits for quantifying the performance of triboelectric nanogenerators, *Nat. Commun.* (2015), <https://doi.org/10.1038/ncomms9376>.
- [36] L. Dhakar, P. Pitchappa, F.E.H. Tay, C. Lee, An intelligent skin based self-powered finger motion sensor integrated with triboelectric nanogenerator, *Nano Energy* 19 (2016) 532–540, <https://doi.org/10.1016/j.nanoen.2015.04.020>.
- [37] Self-powered gait pattern-based identity recognition by a soft and stretchable triboelectric band, *Nano Energy* 56 (2019) 516–523, <https://doi.org/10.1016/J.NANOEN.2018.11.078>.
- [38] X. Meng, Q. Cheng, X. Jiang, Z. Fang, X. Chen, S. Li, C. Li, C. Sun, W. Wang, Z. L. Wang, Triboelectric nanogenerator as a highly sensitive self-powered sensor for driver behavior monitoring, *Nano Energy* 51 (2018) 721–727, <https://doi.org/10.1016/j.nanoen.2018.07.026>.
- [39] Y. Zou, P. Tan, B. Shi, H. Ouyang, D. Jiang, Z. Liu, H. Li, M. Yu, C. Wang, X. Qu, L. Zhao, Y. Fan, Z.L. Wang, Z. Li, A bionic stretchable nanogenerator for underwater sensing and energy harvesting, *Nat. Commun.* 10 (2019) 2695, <https://doi.org/10.1038/s41467-019-10433-4>.
- [40] L. Jin, J. Tao, R. Bao, L. Sun, C. Pan, Self-powered real-time movement monitoring sensor using triboelectric nanogenerator technology, *Sci. Rep.* 7 (2017) 10521, <https://doi.org/10.1038/s41598-017-10990-y>.
- [41] Z. Lin, J. Yang, X. Li, Y. Wu, W. Wei, J. Liu, J. Chen, J. Yang, Large-Scale and washable smart textiles based on triboelectric nanogenerator arrays for self-powered sleeping monitoring, *Adv. Funct. Mater.* 28 (2018) 1704112, <https://doi.org/10.1002/adfm.201704112>.
- [42] S.B. Jeon, Y.H. Nho, S.J. Park, W.G. Kim, I.W. Tcho, D. Kim, D.S. Kwon, Y.K. Choi, Self-powered fall detection system using pressure sensing triboelectric nanogenerators, *Nano Energy* 41 (2017) 139–147, <https://doi.org/10.1016/j.nanoen.2017.09.028>.
- [43] G. Piscitelli, V. Errico, M. Ricci, F. Giannini, G. Saggio, A. Leoni, V. Stornelli, G. Ferri, L. Pantoli, I. Ulisse, A low-cost energy-harvesting sensory headwear useful for tetraplegic people to drive home automation, *AEU - Int. J. Electron. Commun.* 107 (2019) 9–14, <https://doi.org/10.1016/J.AEUE.2019.05.015>.
- [44] Y. Rabhi, M. Mrabet, F. Fnaiech, A facial expression controlled wheelchair for people with disabilities, *Comput. Methods Program. Biomed.* 165 (2018) 89–105, <https://doi.org/10.1016/J.CMPB.2018.08.013>.
- [45] A.M. Choudhari, P. Porwal, V. Jonnalagedda, F. Mériaudeau, An electrooculography based human machine interface for wheelchair control, *Biocybern. Biomed. Eng.* 39 (2019) 673–685, <https://doi.org/10.1016/J.BBE.2019.04.002>.
- [46] L. Wei, H. Hu, Y. Zhang, Fusing EMG and visual data for hands-free control OF an intelligent wheelchair, *Int. J. Humanoid Rob.* (2011) 707–724, <https://doi.org/10.1142/S0219843611002629>, 08.
- [47] S.K. Ameri, M. Kim, I.A. Kuang, W.K. Perera, M. Alshiekh, H. Jeong, U. Topcu, D. Akinwande, N. Lu, Imperceptible electrooculography graphene sensor system for human-robot interface, *Npj 2D Mater. Appl.* 2 (2018) 19, <https://doi.org/10.1038/s41699-018-0064-4>.
- [48] H. Yang, Y. Pang, T. Bu, W. Liu, J. Luo, D. Jiang, C. Zhang, Z.L. Wang, Triboelectric micromotors actuated by ultralow frequency mechanical stimuli, *Nat. Commun.* 10 (2019) 2309, <https://doi.org/10.1038/s41467-019-10298-7>.
- [49] Y. Lee, S.H. Cha, Y.-W. Kim, D. Choi, J.-Y. Sun, Transparent and attachable ionic communicators based on self-cleaneable triboelectric nanogenerators, *Nat. Commun.* 9 (2018) 1804, <https://doi.org/10.1038/s41467-018-03954-x>.
- [50] F. Xi, Y. Pang, W. Li, T. Bu, J. Zhao, G. Liu, T. Guo, W. Liu, C. Zhang, Triboelectric bipolar junction transistor for mechanical frequency monitoring and use as touch switch, *Microsyst. Nanoeng.* 4 (2018) 25, <https://doi.org/10.1038/s41378-018-0026-1>.
- [51] Y.-C. Lai, J. Deng, S.L. Zhang, S. Niu, H. Guo, Z.L. Wang, Single-thread-based wearable and highly stretchable triboelectric nanogenerators and their applications in cloth-based self-powered human-interactive and biomedical sensing, *Adv. Funct. Mater.* 27 (2017) 1604462, <https://doi.org/10.1002/adfm.201604462>.

- [52] T. Chen, Q. Shi, K. Li, Z. Yang, H. Liu, L. Sun, J.A. Dziuban, C. Lee, Investigation of position sensing and energy harvesting of a flexible triboelectric touch pad, *Nanomaterials* (2018) 8, <https://doi.org/10.3390/nano8080613>, Basel, Switzerland.
- [53] B. Meng, W. Tang, Z. Too, X. Zhang, M. Han, W. Liu, H. Zhang, A transparent single-friction-surface triboelectric generator and self-powered touch sensor, *Energy Environ. Sci.* 6 (2013) 3235, <https://doi.org/10.1039/c3ee42311e>.
- [54] X. Pu, H. Guo, J. Chen, X. Wang, Y. Xi, C. Hu, Z.L. Wang, Eye motion triggered self-powered mechnosensational communication system using triboelectric nanogenerator, *Sci. Adv.* 3 (2017), e1700694, <https://doi.org/10.1126/sciadv.1700694>.
- [55] B. Zhang, Y. Tang, R. Dai, H. Wang, X. Sun, C. Qin, Z. Pan, E. Liang, Y. Mao, Breath-based human-machine interaction system using triboelectric nanogenerator, *Nano Energy* 64 (2019) 103953, <https://doi.org/10.1016/J.NANOEN.2019.103953>.
- [56] Z. Lin, J. Chen, X. Li, Z. Zhou, K. Meng, W. Wei, J. Yang, Z.L. Wang, Triboelectric nanogenerator enabled body sensor network for self-powered human heart-rate monitoring, *ACS Nano* 11 (2017) 8830–8837, <https://doi.org/10.1021/acsnano.7b02975>.
- [57] H. Ouyang, J. Tian, G. Sun, Y. Zou, Z. Liu, H. Li, L. Zhao, B. Shi, Y. Fan, Y. Fan, Z. L. Wang, Z. Li, Self-powered pulse sensor for antidiastole of cardiovascular disease, *Adv. Mater.* 29 (2017) 1703456, <https://doi.org/10.1002/adma.201703456>.
- [58] M.S.U. Rasel, J.Y. Park, A sandpaper assisted micro-structured polydimethylsiloxane fabrication for human skin based triboelectric energy harvesting application, *Appl. Energy* 206 (2017) 150–158, <https://doi.org/10.1016/j.apenergy.2017.07.109>.
- [59] S. Wang, Y. Xie, S. Niu, L. Lin, Z.L. Wang, Freestanding triboelectric-layer-based nanogenerators for harvesting energy from a moving object or human motion in contact and non-contact modes, *Adv. Mater.* 26 (2014) 2818–2824, <https://doi.org/10.1002/adma.201305303>.
- [60] T. Jiang, X. Chen, K. Yang, C. Han, W. Tang, Z.L. Wang, Theoretical Study on Rotary-Sliding Disk Triboelectric Nanogenerators in Contact and Non-contact Modes, (n.d.). doi:10.1007/s12274-016-0997-x.
- [61] Y. Xi, J. Hua, Y. Shi, Noncontact triboelectric nanogenerator for human motion monitoring and energy harvesting, *Nano Energy* 69 (2020), <https://doi.org/10.1016/j.nanoen.2019.104390>.
- [62] M. Shi, H. Wu, J. Zhang, M. Han, B. Meng, H. Zhang, Self-powered wireless smart patch for healthcare monitoring, *Nano Energy* 32 (2017) 479–487, <https://doi.org/10.1016/J.NANOEN.2017.01.008>.
- [63] *Static Electric Fields, Maxwell's Equations*, John Wiley & Sons, Inc., Hoboken, NJ, USA, 2011, pp. 56–103, <https://doi.org/10.1002/9780470549919.ch3>.
- [64] S. Niu, S. Wang, L. Lin, Y. Liu, Y.S. Zhou, Y. Hu, Z.L. Wang, Theoretical study of contact-mode triboelectric nanogenerators as an effective power source, *Energy Environ. Sci.* 6 (2013) 3576–3583, <https://doi.org/10.1039/c3ee42571a>.
- [65] J. Tong, B.C. Patel, Anatomy, Head and Neck, Eye Orbicularis Oculi Muscle, StatPearls Publishing, 2019. <http://www.ncbi.nlm.nih.gov/pubmed/28722936>. (Accessed 29 June 2019).
- [66] *Ocular Adnexa and Lacrimal System*, 2012, pp. 159–181, <https://doi.org/10.1016/B978-1-4377-1926-0.10009-8>.
- [67] O. Khunpisuth, T. Chotchinasri, V. Koschakosai, N. Hnoohom, Driver drowsiness detection using eye-closeness detection, in: 2016 12th Int. Conf. Signal-Image Technol. Internet-Based Syst, IEEE, 2016, pp. 661–668, <https://doi.org/10.1109/SITIS.2016.110>.
- [68] I.B. Bandara, Driver Drowsiness Detection Based on Eye Blink, 2009. <http://collections.crest.ac.uk/9782/>. (Accessed 3 October 2019).
- [69] Y. Zou, P. Tan, B. Shi, H. Ouyang, D. Jiang, Z. Liu, H. Li, M. Yu, C. Wang, X. Qu, L. Zhao, Y. Fan, Z.L. Wang, Z. Li, A bionic stretchable nanogenerator for underwater sensing and energy harvesting, *Nat. Commun.* 10 (2019) 2695, <https://doi.org/10.1038/s41467-019-10433-4>.
- [70] R. Zhou, P. Li, Z. Fan, D. Du, J. Ouyang, Stretchable heaters with composites of an intrinsically conductive polymer, reduced graphene oxide and an elastomer for wearable thermotherapy, *J. Mater. Chem. C* 5 (2017) 1544–1551, <https://doi.org/10.1039/C6TC04849H>.



David Vera received his Bachelor degree in Electronic Engineering from the Department of Electrical and Electronic Engineering at North University “Universidad Del Norte” of Barranquilla, Colombia in 2016. He is currently pursuing his Ph.D degree with the Department of Electrical and Computer Systems at Monash University in Melbourne, Australia. His Research interests include energy harvesting systems targeted to biomedical applications, triboelectric nanogenerators, wireless sensor networks and wearable and self-powered sensors.



Tianyi He received her B.Eng. degree from the School of Microelectronics and Solid-state Electronics at the University of Electronic Science and Technology of China (UESTC), Chengdu, China, in 2016. She is now a Ph.D. candidate in the Department of Electrical and Computer Engineering, National University of Singapore. Her research interests include energy harvesters, triboelectric nanogenerator, thermoelectric energy harvester, and wearable sensors.



Chengkuo Lee received his Ph.D. degree in Precision Engineering from The University of Tokyo in 1996. Currently, he is the director of Center for Intelligent Sensors and MEMS at National University of Singapore, Singapore. He was a Senior Member of IEEE. He has contributed to more than 300 peer-reviewed international journal articles. His ORCID is 0000-0002-8886-3649.



Mehmet Rasit Yuce received the M.S. degree in electrical and computer engineering from the University of Florida, Gainesville, FL, in 2001, and the Ph.D. degree in electrical and computer engineering from North Carolina State University, Raleigh, NC, in 2004. In 2011, he joined the Department of Electrical and Computer Systems Engineering, Monash University, Australia. His research interests include wearable devices, wireless implantable telemetry, wireless body area network, biosensors, and integrated circuit technology dealing with digital, analog, and radio frequency circuit designs for wireless, biomedical, and RF applications. He has published more than 100 technical articles in the above areas.